Design of a high performance selective solar absorber with the structure of SiO2 -TiO2 -TiNxOy -Cu

Zhang, Jun; Chen, Tu Pei; Liu, Yu Chan; Liu, Zhen; Yang, Hui Ying

2016

Zhang, J., Chen, T. P., Liu, Y. C., Liu, Z., & Yang, H. Y. (2016). Design of a high performance selective solar absorber with the structure of SiO 2 -TiO 2 -TiN x O y -Cu. ECS Journal of Solid State Science and Technology, 5(7), N43-N47. doi:10.1149/2.0241607jss

https://hdl.handle.net/10356/87282

https://doi.org/10.1149/2.0241607jss

ECS Journal of Solid State Science and Technology, **5** (7) N43-N47 (2016)
2162-8769/2016/5(7)/N43/5/$33.00 © The Electrochemical Society

Design of a High Performance Selective Solar Absorber with the Structure of SiO_2-TiO_2-TiN_xO_y-Cu

J. Zhang,[a] T. P. Chen,[a,z] Y. C. Liu,[b] Z. Liu,[c] and H. Y. Yang[d]

[a]*School of Electrical and Electronic Engineering, Nanyang Technological University, 639798 Singapore*
[b]*Singapore Institute of Manufacturing Technology, 638705 Singapore*
[c]*School of Materials and Energy, Guangdong University of Technology, Guangzhou 510006, People's Republic of China*
[d]*Pillar of Engineering Product Development, Singapore University of Technology and Design, 487372 Singapore*

Using TiN_xO_y thin film as the absorbing layer, a spectrally selective solar absorber (SSA) with the structure of SiO_2-TiO_2-TiN_xO_y-Cu has been designed; and the SSA performance has been evaluated by both calculation and experiment. The TiN_xO_y layer is fabricated by RF magnetron sputtering of a pure TiN target with Ar and N_2 gases. The introduction of oxygen in the TiN_xO_y is realized by using the residual oxygen in the deposition chamber. It is found that the N_2 flow rate has a large effect on the complex refractive index of the TiN_xO_y thin film and thus the SSA performance can be optimized by controlling the N_2 flow rate. With the TiN_xO_y absorbing layer deposited with the N_2 flow rate of 2 sccm, the SSA achieves the highest solar thermal conversion efficiency for a solar radiation concentration factor of equal to or larger than 5. The SSA based on the TiN_xO_y layer deposited with the N_2 flow rate of 2 sccm has a solar absorbance of 96.29% and a thermal emittance of 6.11% at the temperature of 400 °C.

Manuscript submitted May 6, 2016; revised manuscript received June 2, 2016. Published June 14, 2016.

Being the most abundant source of renewable energy, the solar energy resource exceeds all other renewable and fossil-based energy resources combined.[1] One of the direct ways to harvest the solar energy is to convert the solar energy into thermal energy, such as in the cases of solar water heater, solar thermo-photovoltaics, and concentrated solar power (CSP). CSP offers some unique advantages such as higher energy-conversion efficiency, higher thermal energy storage capability, and the potential to retrofit current coal power plants.[2] In a CSP system, the solar absorber has to maximally absorb solar energy while minimizing losses due to black body emission.[2–4]

Different types of selective solar absorber (SSA), such as semiconductor-metal tandems, metal-dielectric multi-layers and conductor-dielectric composites, etc. have been reported.[5] Due to its good thermal stability, high solar absorbance, and low infrared emittance, TiN_xO_y has been studied as solar absorbing layer.[6–8] Because the TiN_xO_y thin film can be treated as the composite of TiN and TiO_2,[9] the conductive TiN serves as the absorption center while the TiO_2 is used as the dielectric host. This is similar to a cermet, such as W-Al_2O_3,[10] Cr-Cr_2O_3,[11] Mo-Si_3N_4,[12] in which the metal nanoparticles are dispersed in the dielectric matrix. For TiN_xO_y films, their optical properties can be tuned by adjusting the N/O ratio of the films;[6,13,14] for example, it was reported that optical properties of the TiN_xO_y films fabricated by reactive mid-frequency magnetron sputtering from titanium nitride target can be controlled in terms of the reactive gas flow rate.[6] This adds the flexibility to optimize the performance of solar absorber.

In this work, a high performance spectrally selective solar absorber (SSA) with the structure of SiO_2-TiO_2-TiN_xO_y-Cu has been designed by tuning the optical properties of the TiN_xO_y absorbing layer in terms of the N_2 flow rate used in the sputtering deposition of the TiN_xO_y layer. The TiN_xO_y absorbing layer is fabricated by RF magnetron sputtering of a pure TiN target with Ar and N_2 gases together with the residual oxygen in the deposition chamber. It is found that the optical properties in a wide spectral region from ultra-violet (UV) to infrared of the TiN_xO_y layer can be significantly changed by changing the N_2 flow rate as a result of the change in the chemical stoichiometry of the TiN_xO_y layer. It is shown that the refractive index and extinction coefficient of the TiN_xO_y layer can be easily tuned to maximize the SSA performance in the wide spectral region by varying the N_2 flow rate. This provides a simple but effective way for the design of a high performance SSA. With the TiN_xO_y absorbing layer deposited with the N_2 flow rate of 2 sccm, the SSA achieves the highest solar thermal conversion efficiency for a solar radiation concentration factor of equal to or larger than 5. The SSA based on the TiN_xO_y layer deposited with the N_2 flow rate of 2 sccm has a solar absorbance of 96.29% and a thermal emittance of 6.11% at the temperature of 400°C.

Experimental

The SSA has the structure of SiO_2-TiO_2-TiN_xO_y-Cu as shown in Figure 1. In this structure, the Cu substrate with high thermal conductivity is utilized as the infrared reflector; the TiN_xO_y film serves as the absorbing layer; and the SiO_2 and TiO_2 thin films form a double-layer anti-reflection coating (ARC). The SiO_2, TiO_2, and TiN_xO_y thin films were deposited by RF magnetron sputtering of 2 inch SiO_2, TiO_2 and TiN targets (all the targets have a purity > 99.9%), respectively, with a magnetron sputtering system (Denton Desktop Pro.). The chamber was pumped down to 9×10^{-6} Torr for all the deposition processes. The sputtering was carried out at room temperature, and the sputtering power was maintained at 100 W. The Ar/O_2 gases were used to deposit SiO_2 and TiO_2 thin films with the O_2 flow rate of 1.5 sccm. The TiN_xO_y thin films used in the SSA were deposited by Ar/N_2 gases with N_2 flow rate at 2, 5, 8 sccm, respectively. The flow rate of Ar was kept at a constant value of 10 sccm, and the deposition pressure was maintained at around 3×10^{-3} Torr. The chemical composition of the TiN_xO_y thin films were examined with an X-ray photoelectron spectroscopy (XPS) system (ESCALAB 250Xi). The XPS analysis shows that the Ti-O, Ti-N-O, and Ti-N states exist in the TiN_xO_y thin films. Figure 2 shows the Ti 2p core level of the two extreme situations of TiN_xO_y thin films, one with 0 sccm N_2 flow rate and another with 9 sccm N_2 flow rate (Ar flow rate was maintained at 10 sccm), which were deposited on silicon substrate for the XPS study. Compared to the TiN_xO_y thin film with 0 sccm N_2 flow rate, the TiN_xO_y thin film with 9 sccm N_2 flow rate has more Ti-O but less Ti-N. This can be explained in the following. The presence of oxygen in the films, which were deposited by sputtering a pure TiN target with Ar/N_2 gases, is due to the existence of residual oxygen in the deposition chamber.[15,16] The presence of oxygen in the TiN_xO_y thin films deposited by a sputtering process without purposeful introduction of O_2 gas was also reported previously.[15,17] It was reported that the deposition rate of the

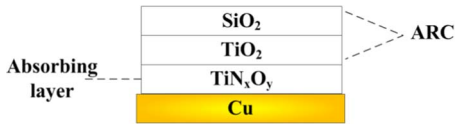

Figure 1. Schematic structure of SSA with SiO_2-TiO_2-TiN_xO_y-Cu.

[z]E-mail: echentp@ntu.edu.sg

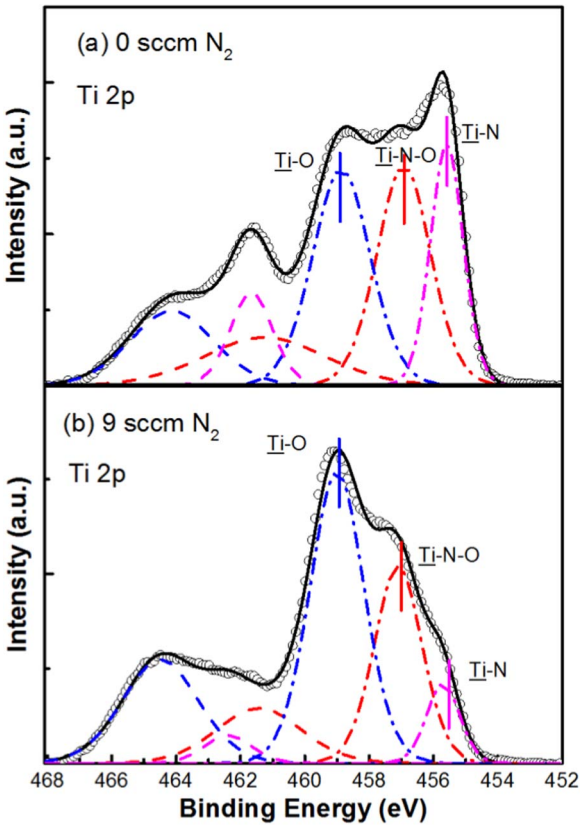

Figure 2. XPS analysis of the Ti 2p core level of the two extreme situation of TiN_xO_y thin films on silicon substrate: (a) deposited with 0 sccm N_2 flow rate; and (b) deposited with 9 sccm N_2 flow rate. In both situations, the Ar flow rate was maintained at 10 sccm.

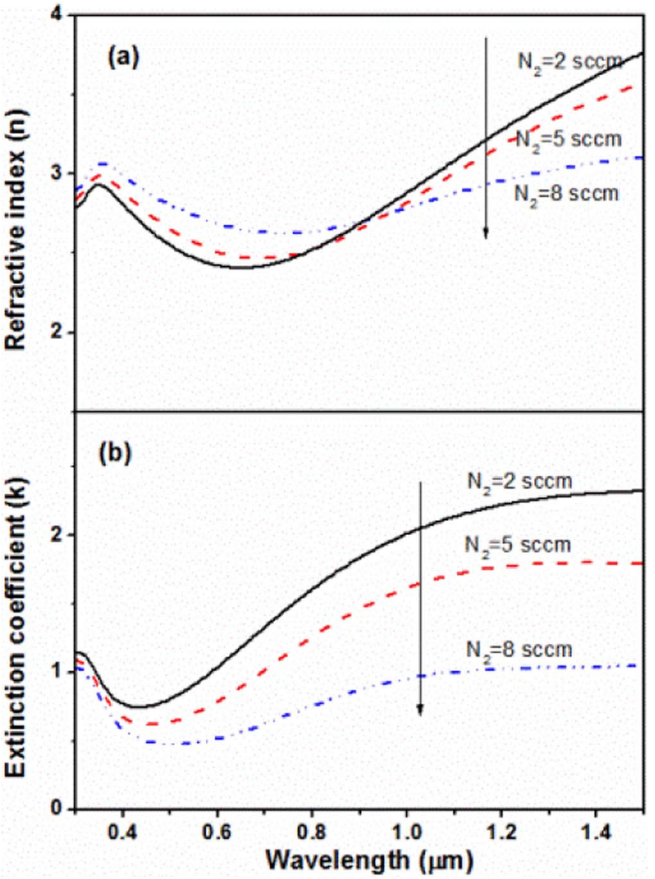

Figure 3. Refractive index and extinction coefficient in the wavelength range of 0.3–1.5 μm of the TiN_xO_y thin films deposited with N_2 flow rates of 2, 5, and 8 sccm, respectively.

TiN_xO_y thin films decreases with increase of N_2 flow rate as a result of the nitriding effect of the TiN target by N_2.[15,18] Also note that oxygen has stronger reaction ability than that of nitrogen with Ti and TiN.[6] With the decrease of deposition rate, the residual oxygen has more time to react with the Ti atoms and thus more oxygen is presented in the deposited films. As a result, there is more Ti-O but less Ti-N in the films deposited with a higher N_2 flow rate. A more detailed XPS examination of the TiN_xO_y thin films is reported elsewhere.[19] The optical properties of TiN_xO_y, TiO_2, and SiO_2 thin films deposited on silicon substrate were measured with spectroscopic ellipsometry (SE). The SE measurements were conducted with a spectroscopic ellipsometer (Woollam VASE) in the wavelength range of 0.3–1.5 μm at the angle of incidence of 75°. Reflectance of the SSA with SiO_2-TiO_2-TiN_xO_y layers deposited on Cu substrate was measured with an UV-Vis-NIR spectrophotometer (PerkinElmer Lambda 950) and a FT-NIR/MIR spectrometer (PerkinElmer Frontier) in the wavelength ranges of 0.3–2.5 μm and 2.5–25 μm, respectively.

Results and Discussion

To design the layer structure of the SSA, the optical properties of the TiN_xO_y layer and the thicknesses of all the layers of the structure must be optimized. Therefore the optical properties of the TiN_xO_y layer must be accurately determined and their dependence on the deposition conditions should be investigated. In this work, the complex dielectric function ($\varepsilon = \varepsilon_r + i\varepsilon_m$, where ε_r and ε_m are the real and imaginary parts of the complex dielectric function (ε), respectively) of the TiN_xO_y thin film is obtained from the SE analysis based on the Drude-Lorentz dispersion model.[20] As the TiN_xO_y film can be considered as a conductive TiN nanoparticles / oxide composite, the Drude-Lorentz dispersion model takes the contributions of the free electrons, localized surface plasmon resonance (LSPR) and interband transitions into account, which are represented by a Drude term and two Lorentz oscillators, respectively. In the fittings based on the Drude-Lorentz dispersion model to the experimental ellipsometric angles, the mean square error (MSE) was utilized as a criteria.[21] The MSE is smaller than 30 for all the SE fittings. Detail of the methodology of the SE analysis is reported elsewhere.[19]

The complex dielectric functions of the TiN_xO_y thin films deposited with various N_2 flow rates have been obtained from the SE analysis in the wavelength range of 0.3–1.5 μm. From the complex dielectric functions, the refractive index (n) and extinction coefficient (k) of the TiN_xO_y thin films are calculated with the following equations:

$$\varepsilon_r = n^2 - k^2 \quad [1]$$

$$\varepsilon_m = 2nk \quad [2]$$

Figure 3 shows the refractive index and extinction coefficient of the TiN_xO_y thin films deposited with N_2 flow rate of 2, 5, 8 sccm, respectively, in the wavelength range of 0.3–1.5 μm. As shown in Figure 3, with the increasing of N_2 flow rate, the refractive index of TiN_xO_y increases in the wavelength range of 0.3–0.9 μm and decreases in the wavelength range of 0.9–1.5 μm. The extinction coefficient decreases significantly as the flow rate of N_2 increases, especially in the infrared range. This indicates that a higher N_2 flow rate will lead to a lower absorption in the TiN_xO_y layer, which is not suitable to the application of TiN_xO_y as the absorbing layer. Nevertheless, the large dependence of both the refractive index and extinction coefficient of the TiN_xO_y layer on the N_2 flow rate may provide an opportunity to optimize the SSA layer structure.

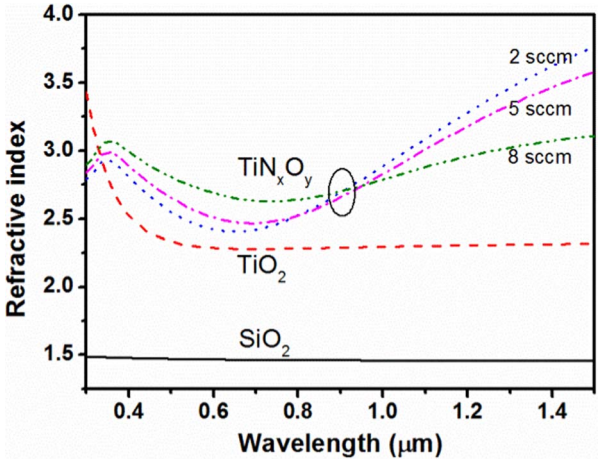

Figure 4. Refractive indexes of SiO_2, TiO_2 and TiN_xO_y thin films in the wavelength range of 0.3–1.5 μm. The TiN_xO_y thin films were deposited with the N_2 flow rates of 2, 5 and 8 sccm, respectively.

In order to achieve a low reflectance in a wide wavelength range (i.e. 0.3–1.5 μm), a graded refractive index profile is usually utilized in a multilayer ARC, which includes low refractive index material (e.g. MgF_2, SiO_2, etc.) and high refractive index material (e.g. TiO_2, Si_3N_4, etc.).[22] In this work, SiO_2 and TiO_2 are chosen to form a double-layer ARC on the TiN_xO_y layer due to their match in the refractive index profile. As shown in Figure 4, a graded refractive index profile, i.e., low refractive index (SiO_2) – medium refractive index (TiO_2) – high refractive index (TiN_xO_y) is indeed achieved in the wide spectrum range of 0.34–1.5 μm.

On the other hand, the refractive indexes and extinction coefficients of TiN_xO_y, TiO_2 and SiO_2 thin films in the infrared range beyond the wavelength of 1.5 μm, which cannot be determined experimentally, can be obtained by the extension of the results shown in Figure 4 using an appropriate optical dispersion model.[19,23,24] With the knowledge of the optical constants in the spectrum range of 0.3–25 μm, a simulation of the reflectance ($R(\lambda)$) of the SiO_2-TiO_2-TiN_xO_y-Cu SSA structure can be carried out to minimize the reflectance in the solar radiation range (i.e. 0.3–1.5 μm) and maximize the reflectance in the infrared range (i.e. 1.5–25 μm) by adjusting the thicknesses of the SiO_2, TiO_2 and TiN_xO_y layers. The optimized thicknesses of the three layers for the N_2 flow rates of 2, 5 and 8 sccm are shown in Figure 5. The total thickness of the three layers is around 180 nm for the N_2 flow rates of 2, 5 and 8 sccm. With the increase of N_2 flow rate from 2 to 8 sccm, the thickness of the absorbing layer (i.e. the TiN_xO_y layer) increases from 57 to 75 nm due to the decrease of the absorption coefficient of TiN_xO_y with increasing N_2 flow rate.

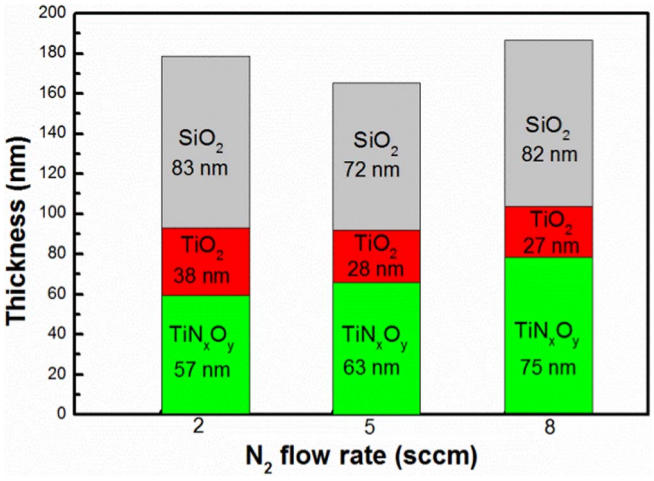

Figure 5. Optimized thicknesses of the SiO_2, TiO_2 and TiN_xO_y layers used in the SSA for the N_2 flow rates of 2, 5 and 8 sccm, respectively.

As the SSA layers are deposited on Cu substrate, the transmittance is zero; thus the solar absorbance ($A_s(\lambda)$) at a specific wavelength (λ) in the solar radiation range can be calculated with Eq. 3.[25] Under the thermal equilibrium condition, the absorbance is equal to the emittance. Therefore the thermal emittance ($E_{bb}(\lambda)$) at a specific wavelength in the infrared radiation range can be obtained with Eq. 4.[26]

$$A_s(\lambda) = 1 - R(\lambda) \quad [3]$$

$$E_{bb}(\lambda) = 1 - R(\lambda) \quad [4]$$

The total solar absorbance (A_{ts}) and total thermal emittance (E_{tbb}) are given by Eq. 5 and Eq. 6, respectively.[27]

$$A_{ts} = \frac{\int_{\lambda=0.3\,\mu m}^{\lambda=\lambda_c} P_{solar}(\lambda) \times A_s(\lambda) d\lambda}{\int_{\lambda=0.3\,\mu m}^{\lambda=\lambda_c} P_{solar}(\lambda) d\lambda} \quad [5]$$

$$E_{tbb} = \frac{\int_{\lambda=\lambda_c}^{\lambda=25\,\mu m} P_{bb}(\lambda) \times E_{bb}(\lambda) d\lambda}{\int_{\lambda=\lambda_c}^{\lambda=25\,\mu m} P_{bb}(\lambda) d\lambda} \quad [6]$$

where $P_{solar}(\lambda)$ is the intensity of the solar radiation (AM 1.5), $P_{bb}(\lambda)$ is the intensity of black body radiation, λ_c is the transition point.

In order to realize high solar absorbance and low thermal emittance, the reflectance should be low in the solar radiation range and high in the infrared range. The transition point between those two regions is at the cross point of the solar radiation spectrum and the blackbody radiation spectrum. In the mid-temperature SSA application (e.g., 400°C), the blackbody radiation exceeds to the solar radiation at the wavelength of 1.5 μm, as shown in Figure 7. On the other hand, around 90% of solar energy is in the wavelength range of 0.3–1.5 μm.[28] Therefore, the transition point (λ_c) in this work is set at the wavelength of 1.5 μm.

With the optimized layer thicknesses shown in Figure 5, the total solar absorbance (A_{ts}) and total thermal emittance (E_{tbb}) of the SSA are calculated with Eq. 5 and Eq. 6, respectively, for N_2 flow rates of 2, 5 and 8 sccm, and the results are shown in Table I. It is found from the table that, with the increase of the N_2 flow rate from 2 to 8 sccm, the A_{ts} decreases from 97.55% to 91.37%, and the E_{tbb} also decreases from 7.27% to 6.56%. The change of A_{ts} with N_2 flow rate can be explained by the change of the chemical stoichiometry of the TiN_xO_y thin films. The XPS analysis shows that the ratio of N to O in the TiN_xO_y layers decreases from 0.49 to 0.21 with the increase of N_2 from 2 to 8 sccm. This means that the amount of the TiN component in the TiN_xO_y layers decreases with N_2 flow rate. The TiN component serves as the absorption center in the TiN_xO_y absorbing layers. Therefore, when the N_2 flow rate increases, A_{ts} decreases with the decrease of the amount of the TiN component. The SSA of the N_2 flow rate of 2 sccm has the largest A_{ts} (97.55%) due to the largest absorption in the TiN_xO_y layer deposited with the N_2 flow rate of 2 sccm. On the other hand, for the N_2 flow rate of 8 sccm, the SSA has the smallest E_{tbb} (6.56%) at the temperature of 400°C.

Table I. A_{ts} and E_{tbb} calculated with Eq. 5 and Eq. 6, respectively for the optimized layer thicknesses shown in Figure 5.

	SSA (N_2 = 2 sccm)	SSA (N_2 = 5 sccm)	SSA (N_2 = 8 sccm)
A_{ts}	97.55%	96.73%	91.37%
E_{tbb}	7.27%	7.10%	6.56%

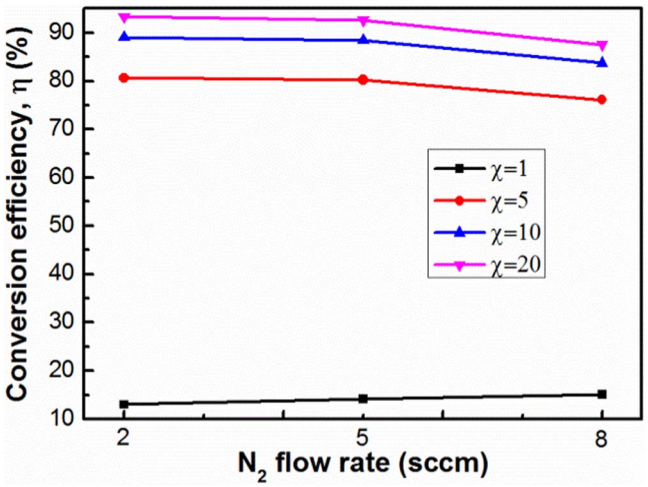

Figure 6. Solar thermal conversion efficiency (η) at the temperature of 400°C as a function of the concentration factor (χ) for the N_2 flow rates of 2, 5 and 8 sccm.

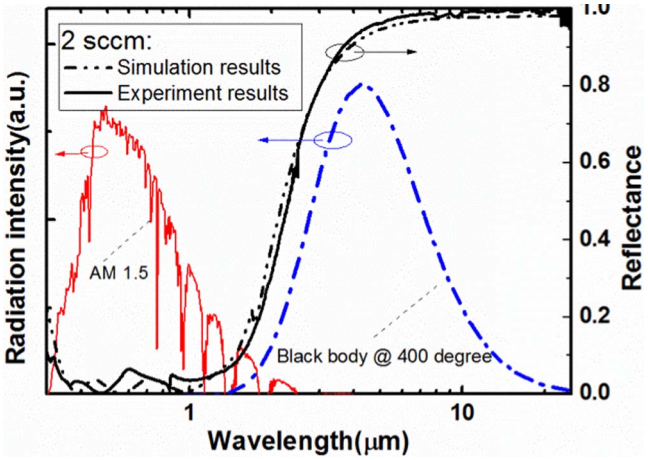

Figure 7. Intensity of solar radiation (AM 1.5), intensity of black body radiation at 400°C, and the simulated and experimental reflectance of the SSA with the TiN_xO_y layer deposited with the N_2 flow rate of 2 sccm.

In order to evaluate the performance of the SSA, the solar thermal conversion efficiency (η) is calculated with Eq. 7.[29]

$$\eta = A_{ts} - \frac{E_{tbb}\sigma T^4}{\chi P_{solar}} \quad [7]$$

where σ is the Stefan-Boltzmann constant (5.6696×10^{-8} $W \cdot m^{-2} \cdot K^{-4}$); T is the absolute temperature; χ is the solar concentration factor; P_{solar} is the total solar radiation intensity. According to Eq. 7, the solar thermal conversion efficiency (η) depends on the concentration factor (χ). The solar thermal conversion efficiency at the temperature of 400°C as a function of the concentration factor is calculated with Eq. 7 for N_2 flow rates of 2, 5 and 8 sccm, respectively, and the result is shown in Figure 6. When χ is one, η is 13.00%, 14.16%, and 15.08%, for the N_2 flow rates of 2, 5 and 8 sccm, respectively, showing a very low η. When χ is 5, there is a large increase in η, i.e., η is 80.64%, 80.22% and 76.11% for the N_2 flow rates of 2, 5 and 8 sccm, respectively. It can be observed from Figure 6 that the N_2 flow rate of 2 sccm provides the highest η for χ equal to or larger than 5. In the mid-high temperature SSA applications, the solar energy usually is concentrated on the absorber with parabolic tough with χ of larger than 10.[30,31] Therefore, the N_2 flow rate of 2 sccm has been chosen to deposit the TiN_xO_y absorbing layer in the fabrication of the mid-high temperature (i.e. 400°C) SSA with the structure of SiO_2-TiO_2-TiN_xO_y-Cu in this work.

The reflectance of the fabricated SSA with the N_2 flow rate of 2 sccm has been measured in the wavelength range of 0.3–25 μm, and the result is compared with the simulation in Figure 7. As shown in Figure 7, the experiment agrees well with the simulation in the large wavelength range of 0.3–25 μm. The SSA has a low reflectance (<0.1) in the wavelength range of 0.3–1.5 μm (i.e. the solar radiation range) and high reflectance in the wavelength range of 1.5–25 μm (i.e. the black body radiation range at 400°C). The measured solar absorbance and thermal emittance at the temperature of 400°C of the fabricated SSA are 96.29% and 6.11%, respectively, which agree well with the calculation discussed early (the calculated solar absorbance and thermal emittance at the temperature of 400°C are 97.55% and 7.27%, respectively).

Conclusions

By using TiN_xO_y as the absorbing layer, a high performance SSA with the structure of SiO_2-TiO_2-TiN_xO_y coating on Cu substrate has been designed and fabricated. The SiO_2 and TiO_2 layers form a double-layer ARC while the Cu substrate serves as infrared reflector. The TiN_xO_y layer was deposited by sputtering of a pure TiN target with Ar and N_2. Introducing of oxygen in the TiN_xO_y layer was realized by utilizing the residual oxygen in the deposition chamber. The N_2 flow rate has a large effect on the optical properties of the TiN_xO_y layer; and with the increase of the N_2 flow rate, the extinction coefficient of the TiN_xO_y layer decreases significantly. Based on the optical properties of the TiN_xO_y layer obtained from the SE analysis, the thicknesses of the SiO_2, TiO_2 and TiN_xO_y layers are optimized to achieve the highest total solar absorbance and the lowest total thermal emittance for a given N_2 flow rate. The N_2 flow rate of 2 sccm provides the highest solar thermal conversion efficiency for the concentration factor equal to or larger than 5. The SSA fabricated with the N_2 flow rate of 2 sccm shows a high solar absorbance of 96.29% and a low thermal emittance of 6.11% at the temperature of 400°C.

Acknowledgments

This work is financially supported by the National Research Foundation (Program grant No. NRF-CRP13-2014-02) and NTU-A*STAR Silicon Technologies Centre of Excellence (Program grant No. 112 3510 0003). Z. Liu acknowledge the support by NSFC under Project No. 61404031.

References

1. N. S. Lewis, "Toward Cost-Effective Solar Energy Use," *Science*, **315**, 798 (2007).
2. J. Moon, D. Lu, B. VanSaders, T. K. Kim, S. D. Kong, S. Jin, R. Chen, and Z. Liu, "High performance multi-scaled nanostructured spectrally selective coating for concentrating solar power," *Nano Energy*, **8**, 238 (2014).
3. F. Cao, K. McEnaney, G. Chen, and Z. Ren, "A review of cermet-based spectrally selective solar absorbers," *Energy Environ. Sci.*, **7**, 1615 (2014).
4. H. C. Barshilia, P. Kumar, K. S. Rajam, and A. Biswas, "Structure and optical properties of Ag-Al_2O_3 nanocermet solar selective coatings prepared using unbalanced magnetron sputtering," *Sol. Energy Mater. Sol. Cells*, **95**, 1707 (2011).
5. N. Selvakumar and H. C. Barshilia, "Review of physical vapor deposited (PVD) spectrally selective coatings for mid- and high-temperature solar thermal applications," *Sol. Energy Mater. Sol. Cells*, **98**, 1 (2012).
6. F. Chen, S.-W. Wang, L. Yu, X. Chen, and W. Lu, "Control of optical properties of TiN_xO_y films and application for high performance solar selective absorbing coatings," *Opt. Mater. Express*, **4**, 1833 (2014).
7. M. Lazarov, B. Röhle, T. Eisenhammer, and R. Sizmann, "TiN_xO_y-Cu Coatings for Low Emissive Solar Selective Absorbers," 1536, p. 183–191, The Society of Photo-optical Instrumentation Engineers Proceedings, San Diego, CA (1991).
8. H. Schellinger, M. P. Lazarov, H. Klank, and R. Sizmann, "Thermal and Chemical Metallic - Dielectric Transitions of TiN_xO_y Cu Absorber Tandems," *SPIE's 1993 Int. Symp. Opt. Imaging, Instrum.*, **2077**, 366 (1993).
9. D. A. Duarte, J. C. Sagás, A. S. Da Silva Sobrinho, and M. Massi, "Modeling the reactive sputter deposition of N-doped TiO_2 for application in dye-sensitized solar cells: Effect of the O_2 flow rate on the substitutional N concentration," *Appl. Surf. Sci.*, **269**, 55 (2013).

10. A. Antonaia, A. Castaldo, M. L. Addonizio, and S. Esposito, "Stability of W-Al_2O_3 cermet based solar coating for receiver tube operating at high temperature," *Sol. Energy Mater. Sol. Cells*, **94**, 1604 (2010).
11. V. Teixeira, E. Sousa, M. F. Costa, C. Nunes, L. Rosa, M. J. Carvalho, M. Collares-Pereira, E. Roman, and J. Gago, "Spectrally selective composite coatings of Cr-Cr_2O_3 and Mo-Al_2O_3 for solar energy applications," *Thin Solid Films*, **392**, 320 (2001).
12. E. Céspedes, M. Wirz, J. A. Sánchez-García, L. Alvarez-Fraga, R. Escobar-Galindo, and C. Prieto, "Novel Mo-Si_3N_4 based selective coating for high temperature concentrating solar power applications," *Sol. Energy Mater. Sol. Cells*, **122**, 217 (2014).
13. S. J. Cho, C. K. Jung, and J. H. Boo, "A study on the characteristics of TiO_xN_y thin films with various nitrogen flow rate by PECVD method," *Curr. Appl. Phys.*, **12**, S29 (2012).
14. S. H. Mohamed, O. Kappertz, J. M. Ngaruiya, T. Niemeier, R. Drese, R. Detemple, M. M. Wakkad, and M. Wuttig, "Influence of nitrogen content on properties of direct current sputtered TiO_xN_y films," *Phys. Status Solidi Appl. Res.*, **201**, 90 (2004).
15. N. White, A. L. Campbell, J. T. Grant, R. Pachter, K. Eyink, R. Jakubiak, G. Martinez, and C. V. Ramana, "Surface/interface analysis and optical properties of RF sputter-deposited nanocrystalline titanium nitride thin films," *Appl. Surf. Sci.*, **292**, 74 (2014).
16. N. K. Ponon, D. J. R. Appleby, E. Arac, P. J. King, S. Ganti, K. S. K. Kwa, and A. O'Neill, "Effect of deposition conditions and post deposition anneal on reactively sputtered titanium nitride thin films," *Thin Solid Films*, **578**, 31 (2015).
17. C. M. Zgrabik and E. L. Hu, "Optimization of sputtered titanium nitride as a tunable metal for plasmonic applications," *Opt. Mater. Express*, **5**, 478 (2015).
18. S. Wrehde, M. Quaas, R. Bogdanowicz, H. Steffen, H. Wulff, and R. Hippler, "Optical and chemical characterization of thin TiN_x films deposited by DC-magnetron sputtering," *Vacuum*, **82**, 1115 (2008).
19. J. Zhang, T. P. Chen, X. D. Li, Y. C. Liu, Y. Liu, and H. Y. Yang, "An Investigation of Localized Surface Plasmon Resonance of TiN Nanoparticles in TiN_xO_y Thin Films", submitted to *J. Appl. Phys.*
20. N. Delegan, R. Daghrir, P. Drogui, and M. A. El Khakani, "Bandgap tailoring of in-situ nitrogen-doped TiO_2 sputtered films intended for electrophotocatalytic applications under solar light," *J. Appl. Phys.*, **116**, 153510 (2014).
21. V. Stranak, M. Quaas, R. Bogdanowicz, H. Steffen, H. Wulff, Z. Hubicka, M. Tichy, and R. Hippler, "Effect of nitrogen doping on TiO_xN_y thin film formation at reactive high-power pulsed magnetron sputtering," *J. Phys. D. Appl. Phys.*, **43**, 285203 (2010).
22. J. Zhang, T. P. Chen, Y. Liu, and J. I. Wong, "Si nanocrystal-based triple-layer anti-reflection coating for Si solar cells," *J. Appl. Phys.*, **114**, 053109 (2013).
23. G. Droulers, A. Beaumont, J. Beauvais, and D. Drouin, "Spectroscopic ellipsometry on thin titanium oxide layers grown on titanium by plasma oxidation," *J. Vac. Sci. Technol. B Microelectron. Nanom. Struct.*, **29**, 021010 (2011).
24. M. Jerman, Z. Qiao, and D. Mergel, "Refractive index of thin films of SiO_2, ZrO_2, and HfO_2 as a function of the films' mass density," *Appl. Opt.*, **44**, 3006 (2005).
25. J. Chen, C. Guo, J. Chen, J. He, Y. Ren, and L. Hu, "Microstructure, optical and electrical properties of CrAlN film as a novel material for high temperature solar selective absorber applications," *Mater. Lett.*, **133**, 71 (2014).
26. N. Selvakumar, S. B. Krupanidhi, and H. C. Barshilia, "Carbon nanotube-based tandem absorber with tunable spectral selectivity: Transition from near-perfect blackbody absorber to solar selective absorber," *Adv. Mater.*, 2552 (2014).
27. K. Valleti, D. Murali Krishna, and S. V. Joshi, "Functional multi-layer nitride coatings for high temperature solar selective applications," *Sol. Energy Mater. Sol. Cells*, **121**, 14 (2014).
28. Louis Spanoudis, "Solar energy collector having solar selective coating of low reflectance", United States Pat., 4334523 (1982).
29. H. J. Brown-Shaklee, W. Carty, and D. D. Edwards, "Spectral selectivity of composite enamel coatings on 321 stainless steel," *Sol. Energy Mater. Sol. Cells*, **93**, 1404 (2009).
30. H. L. Zhang, J. Baeyens, J. Degrève, and G. Cacères, "Concentrated solar power plants: Review and design methodology," *Renew. Sustain. Energy Rev.*, **22**, 466 (2013).
31. O. Behar, A. Khellaf, and K. Mohammedi, "A review of studies on central receiver solar thermal power plants," *Renew. Sustain. Energy Rev.*, **23**, 12 (2013).